ELSEVIER

Earth and Planetary Science Letters 148 (1997) 27–43

EPSL

Grain-size evolution in subducted oceanic lithosphere associated with the olivine–spinel transformation and its effects on rheology

Michael R. Riedel [a,*], Shun-ichiro Karato [b]

[a] *Project Group Thermodynamics, University of Potsdam, D-14473 Potsdam, Germany*
[b] *Department of Geology and Geophysics, University of Minnesota, Minneapolis, MN 55455, USA*

Received 6 June 1996; accepted 22 January 1997

Abstract

We investigate the role of grain-size reduction during the olivine–spinel transformation on rheological properties of subducting slabs on the basis of a scaling model for microstructural development during nucleation and growth. In this model, the size of spinel grains nucleating at olivine grain boundaries is controlled by the relative rates of nucleation and growth, taking into account the impingement through the collision of grains due to growth. When the volume fraction of spinel reaches a certain threshold value (critical volume fraction ~ 1–10%, depending on the P–T conditions in the slab), the new phase will form a continuous film and will significantly reduce the strength of the two-phase aggregate, if spinel grain size is small. The size of spinel grains, δ_0, at this stage is calculated and is shown to be highly sensitive to temperature. At relatively high temperatures ($T > 1000$ K), δ_0 shows an Arrhenius-type dependence on temperature; that is, $\delta_0 \sim \exp(-E^*/RT)$ with $E^* \sim 400$ kJ/mol, whereas a more complicated temperature dependence is found at low temperatures ($T < 900$ K), where a grain-size reduction of up to 4 orders in magnitude is possible.

Strength profiles of slabs due to combined effects of temperatures and of grain-size reduction are calculated. It is shown that: (1) the strength of slabs will have an unusual temperature dependence through the temperature dependence of grain size; and (2) a subducting slab has a complicated rheological structure containing a weak region below the tip of a metastable olivine-bearing wedge in a cold slab. Possible implications of these anomalous rheological structures of slabs on the dynamics of subduction are discussed, including the mechanisms of deep earthquakes.

Keywords: subduction zones; rheology; phase transitions; deep-focus earthquakes; grain size; kinetics

1. Introduction

Subducted oceanic lithosphere appears to have a diversity of interaction with the mantle transition zone, which results in a complex chemical evolution and convective pattern of the Earth's mantle. An important factor that controls the fate of subducted lithosphere is its creep strength, to which grain-size reduction and latent heat release, associated with the olivine–spinel transformation might contribute important effects. The effects due to grain-size reduction can potentially be large because rheological properties of Earth materials are highly sensitive to grain size when grain size becomes sufficiently small [1–3].

Earlier studies suggested significant weakening of slabs due to grain-size reduction, based on laboratory

* Corresponding author. E-mail: miker@gfz-potsdam.de

PII S0012-821X(97)00016-2

observations of small grain sizes after phase transformations [1,2,4,5]. A major limitation of these previous studies, however, is the fact that grain-size reduction was observed at laboratory time scales where large driving forces for phase transformation(s) are applied to achieve a significant transformation within reasonable laboratory times (a few hours). Phase transformations in the Earth, such as in subducting slabs, occur at much longer time scales with either much smaller driving forces or at much lower temperatures. Thus, grain size after transformations in subducting slabs could be significantly different from those observed in high-pressure experiments, and the observation of small grain size in the laboratory does not necessarily imply significant grain-size reduction in the Earth's mantle. The central question then arises of how to estimate likely grain sizes for geologically relevant time scales from laboratory data.

Recently, Riedel and Karato [6] have developed a theoretical model for assessing the scaling laws of grain-size evolution during first-order phase transformations. Here, we apply this theoretical framework to estimate the grain sizes during and after the olivine–spinel transformation in subducting slabs, and, in addition, we estimate the effects of grain–size reduction on the rheological structure of slabs. For this purpose, we have also taken into account the temperature feedback from the latent heat release associated with the transformation. We assume that the rheology of peridotite is controlled either by the rheology of olivine, the weakest and most abundant mineral in the upper mantle [7,8], or by that of its high-pressure polymorphs β- or γ-spinel. In the two-phase region, we use a phenomenological flow law [9] to estimate the creep strength of mixed aggregates of olivine and spinel. The degree of phase transformation inside the slab is calculated on the basis of the available experimental data on the olivine–spinel transition kinetics (a compilation is given, e.g., in [10]) and the geothermal models of slabs by McKenzie [11,12], and the change in creep strength is calculated on the basis of a representative strain rate of 10^{-15} s^{-1}.

Our results show that spinel grain size is highly sensitive to temperature, and a large grain-size reduction and resultant significant rheological weakening is expected for cold slabs but not for warm slabs. Instead of a strong elastic ''core'', we find the development of a weak zone below the tip of a metastable olivine-bearing wedge in cold slabs, implying a rheological separation of the slab into two comparatively strong regions between 450 km and 600 km depth. As a result, the overall strength of a cold slab could become lower than the strength of a warm slab.

2. Thermal structure of subducted slabs and phase transformation kinetics

The thermal structure of subducting slabs depends primarily on the rate of subduction and on the age of the subducting oceanic lithosphere and therefore varies greatly for different subduction zones (see, e.g., [13,14]). Minimum predicted slab temperatures can be as low as 500°C at a depth where the olivine–spinel transition sets in in rapidly subducting slabs of old lithosphere. In younger slabs which subduct at relatively low velocity, the minimum temperature at this depth is likely to be much higher than 500°C. The difference between the P–T conditions inside the slab and those outside is one reason that the slab differs in mineralogy from the equilibrium mantle assemblages outside. The conventional picture of the cold slab implies, in addition, that it should also be mechanically stronger than its surrounding, and thus able to sustain and transmit higher stresses to greater depth (therefore acting as a ''stress guide'').

A simple analytical model for the thermal profile of subduction zones is given by McKenzie's solution [11,12] for a slab of finite thickness L subducting into a hotter isothermal mantle of temperature, T_0, with constant velocity v_{slab}:

$$T(x,z) = T_0 + 2(T_0 - 273)\sum_{n=1}\frac{(-1)^n}{n\pi} \times \exp\left[\left(Re - \sqrt{Re^2 + n^2\pi^2}\right)\frac{x}{L}\right] \times \sin\left(n\pi\frac{z}{L}\right) \quad (1)$$

where: $Re = \rho C_p v_{\mathrm{slab}} L/2\kappa$ is the thermal Reynolds number; ρ is the density; C_p is the specific heat;

κ is the thermal conductivity of the slab material; and the coordinates (x, z) are parallel to the slab width and length, respectively (Fig. 1). According to Eq. (1), isotherms within the slab are advected downward such that the maximum depth, z_{max}, reached by any isotherm is proportional to the product of the vertical descent rate (trench-normal convergence rate times the sine of the dip) and the square of plate thickness, $z_{max} \sim v_{slab} \cdot L^2$.

The main portion of subducted slabs has an olivine-rich mineralogy in the upper mantle. To simplify the analysis, we assume that a subducting slab is composed of 60% olivine and that this component transforms directly into the spinel phase at a certain depth. At low temperatures, where the transformation of olivine close to the equilibrium pressure is kinetically inhibited, direct transformation to either β- or γ-$(Mg, Fe)_2SiO_4$ is likely to occur without any change in composition and therefore without long-range diffusion processes [10]. The growth rate of β or γ in this case may be described by a kinetic equation of the form:

$$Y = Y_0 T \exp\left[-\frac{Q_a + PV_a}{RT}\right]\left\{1 - \exp\left[-\frac{\Delta\mu}{RT}\right]\right\} \quad (2)$$

where: Q_a and V_a are the activation energy and activation volume for diffusion, respectively; R is the gas constant; $\Delta\mu$ is the molar free energy difference between olivine and spinel; and Y_0 is a constant.

It has been shown that the $\alpha \rightarrow \beta$ and $\alpha \rightarrow \gamma$ transition under low (mantle-like) differential stresses of less than about 1 GPa evolves predominantly as a grain-boundary nucleated process; that is, spinel grains nucleate along pre-existing olivine grain boundaries and grow afterwards at the expense of the host olivine [15–17]. The appropriate kinetic rate

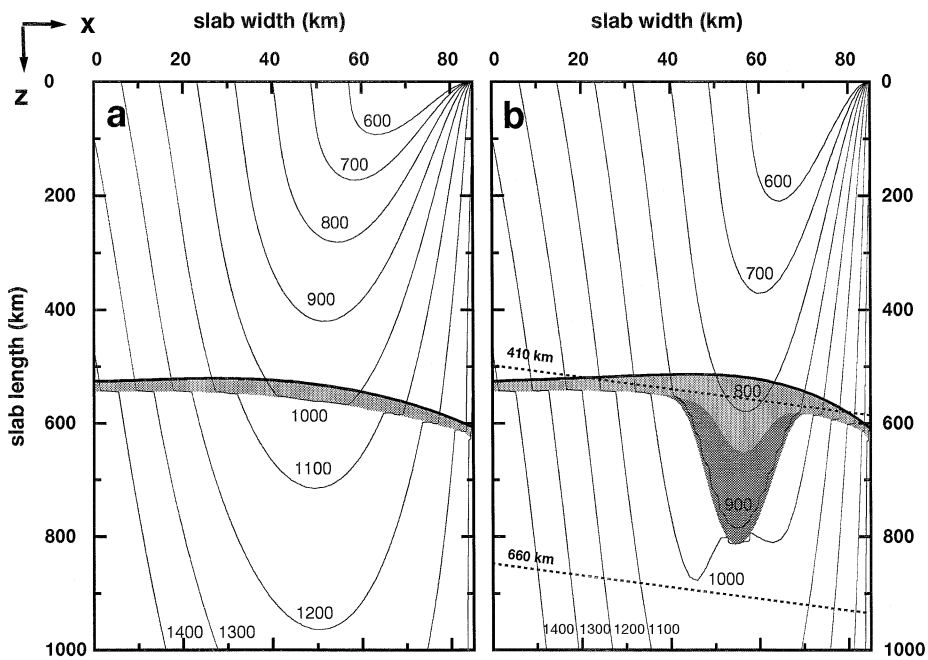

Fig. 1. Slab geometry used for the numerical model. The slab is considered as a rigid body with thickness L and a fixed length of 1000 km. The penetration angle is 45° (upper surface of the slab at the right side). Isotherms (in Kelvin) are calculated using McKenzie's model [11,12], corrected with the latent heat feedback. The bold line shows the phase equilibrium boundary of olivine and β-spinel, according to the thermodynamic data of Akaogi et al. [44] Table 1. (a) $v_{slab} = 4$ cm/yr, $L = 85$ km, $Re = 59.30$. (b) $v_{slab} = 10$ cm/yr, $L = 85$ km, $Re = 148.25$. The metastability region of pure olivine (grey) and the region with mixed olivine–spinel aggregates (dark grey) are shown.

equation for this type of nucleation (compare, e.g., [18]) is:

$$I^B = I_0^B T \exp\left[-\frac{Q_a + PV_a}{RT}\right]\exp\left[-\frac{\eta \cdot \Delta G^*_{\text{hom}}}{kT}\right] \quad (3)$$

where: I_0^B is a pre-exponential constant; k is the Boltzmann constant; ΔG^*_{hom} is the activation energy for the formation of a critical nucleus that depends on the thermodynamic driving force $\Delta\mu$; and η is the shape factor accounting for the lowering of ΔG^*_{hom}, due to the nucleation at pre-existing grain boundaries (see, e.g., [10,19]).

The overall transformation kinetics; that is, the volume fraction of the new phase as a function of time, $\xi(t)$, depend on the rates of both nucleation and growth and are affected by the impingement of the growing grains. $\xi(t)$ is given by [10,18,20]:

$$\xi(t) = 1 - \exp\left\{-2\,{}^{v}O^B \int_0^t \left[1 - \exp\left(-A_e(t,t')\right)\right] \times Y(t')\,\mathrm{d}t'\right\} \quad (4)$$

where: A_e is the increase in the extended area fraction of spinel per unit volume (see appendix for details); and ${}^{v}O^B$ is the grain boundary area per unit volume of olivine. The effect of latent heat release is accounted for by including an additional term in Eq. (1):

$$\Delta T_Q(x,z) = \int_{(x,0)}^{(x,z)} \frac{F_{\text{ol}} Q(x,z')}{\rho C_p v_{\text{slab}}} \left.\frac{d\xi}{\mathrm{d}t}\right|_{(x,z')} \mathrm{d}z' \quad (5)$$

where: $F_{\text{ol}} = 0.6$ is the olivine content in peridotite; Q is the released heat; and $\mathrm{d}\xi/\mathrm{d}t$ is the increase in transformation degree at depth $(x,\ z')$ [10,19,21].

In order to obtain the transformed volume fraction of spinel $\xi(t)$, Eq. (4), we solve the ordinary differential equations given in Appendix A, Eq. (A4) or Eq. (A5), using a 4th-order Runge–Kutta algorithm [22] along a layer of subducting lithosphere for the local P–T conditions. The effect of latent heat, Eq. (5), is added as a correction term to $T(x,\ z > z')$ at each integration step $z' \rightarrow z' + \mathrm{d}z'$ within the slab. We neglect the thermal dissipation of the latent heat

Table 1
Thermo-mechanical slab constants and kinetic parameters

Constant or parameter	Value
Slab thickness, L [43]	60–100 km
Lithosphere base temperature, T_0 [43]	1273 K
Penetration angle of the slab	45°
Heat capacity, C_p [44]	1.0467×10^3 J kg^{-1} K^{-1}
Thermal conductivity, κ [43]	3.14 J m^{-1} s^{-1} K^{-1}
Thermal expansion (0th order α_0) [23]	3.5×10^{-5} K^{-1}
Thermal expansion (1st order α_1) [23]	-1.7×10^{-11} K^{-1} m^{-1}
Adiabatic compressibility, β_a [43]	4.3×10^{-3} GPa^{-1}
Mantle density ρ at $z = 0$ [43]	3.3×10^3 kg m^{-3}
Surface energy, σ [10]	0.6 J m^{-2}
Shape factor for grain-boundary nucleated reaction, η [10]	6×10^{-4}
Activation energy, Q_a [15]	4.00×10^5 J mol^{-1}
Activation volume, V_a [10]	6.1×10^{-6} m^3 mol^{-1}
Entropy difference, ΔS [44]	7.7 J mol^{-1} K^{-1}
Volume change, ΔV [44]	3.16×10^{-6} m^3 mol^{-1}
Clapeyron constant, p_0 (see text) [44]	11.0 GPa
Molar volume of spinel, V_m [44]	4.05×10^{-5} m^3 mol^{-1}
Molar volume of olivine, [44]	4.37×10^{-5} m^3 mol^{-1}
Pre-exponential constant, Y_0 [16] [a]	1.40×10^{10} m s^{-1} K^{-1}
Pre-exponential constant, I_0^B [10]	1.0×10^{37} m^{-2} s^{-1} K^{-1}
Grain-boundary area per unit volume of olivine, ${}^{v}O^B$ [25]	1.0×10^3 m^{-1}

[a] Fujino and Irifune [16] observed the growth of small β-spinel aggregates along the margin of a forsterite single crystal. Taking their fig. 2a with the result of the phase transformation after 20 min, we obtain, as a lower limit for the spinel growth rate, a value of $3.1 \cdot 10^{-8}$ m s^{-1} at 15.5 GPa and 1273 K. This value is used here as a fixed point for the determination of Y_0.

in the slab, since it is slow compared with the transformation kinetics for fast subduction [23] and would lead only to minor corrections of the McKenzie temperature profile (adiabatic heating included). Typically, the equations are integrated along the direction of subduction z within 10000 steps; that is, for a slab of 1000 km length the integration step width is 100 m.

Table 1 contains a compilation of the thermodynamic parameters used for the thermo-kinetic model. Note that the kinetic parameter for the non-equilibrium transition of α-Mg_2SiO_4 to β-phase is still subject to large uncertainties (for respective reviews, see [10,24]).

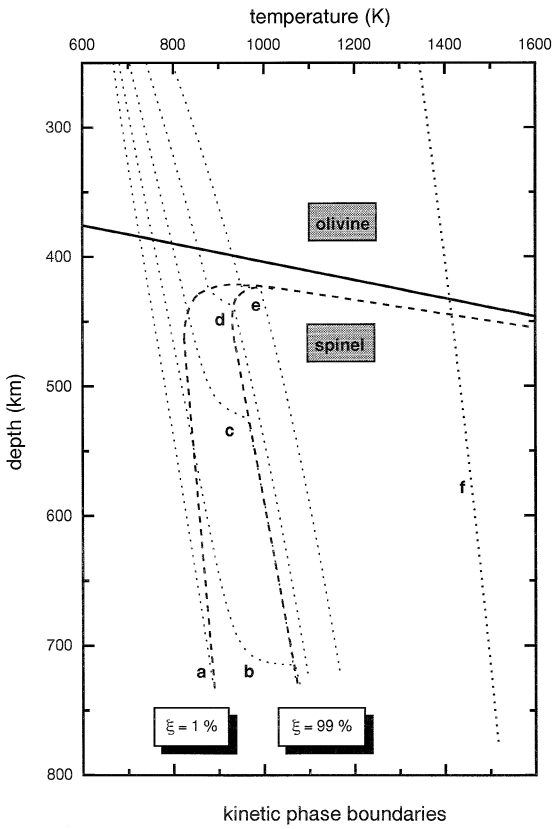

Fig. 2. $P-T$ phase diagram showing the kinetic phase boundaries for 1% and 99% transformation degree (dashed lines). The thick line shows the phase equilibrium of olivine and β-spinel, according to the thermodynamic data of Akaogi et al. [44]. The adiabats a–e represent the $P-T$ paths of the coldest portion of a slab ($v_{slab} = 10$ cm/yr) with different thicknesses: (a) $L = 100$ km; (b) $L = 90$ km; (c) $L = 80$ km; (d) $L = 70$ km; (e) $L = 60$ km; (f) boundary condition of the McKenzie model.

The resulting kinetic phase boundaries (1% and 99% transition degree) are shown in Fig. 1. It can be seen that the thermal structure of a slab is significantly modified by the phase transformation. The non-equilibrium phase boundary of olivine and β-spinel is advected to greater depth (boundary between the region with metastable olivine (grey) and the two-phase region (dark grey)), and the slab temperature is typically increased by 30–130°C. The $P-T$ paths along the central (coldest) portions of slabs with increasing thicknesses are plotted in Fig. 2. As emphasized previously [10], the latent heat production causes the transformation to occur by a runaway process, which results in steep thermal gradients around the metastable olivine wedge below 600 km depth [19].

3. Grain-size evolution in subducting slabs

The fundamental physical processes that control grain sizes during and after a first-order phase transformation have been investigated by Riedel and Karato [6]. New grains are formed on grain boundaries in the case of heterogeneous nucleation, growing subsequently at the expense of the host phase. Upon impingement, their size is fixed, which is therefore controlled by the competition between nucleation and growth. Briefly, grain size is small when nucleation dominates over growth, and vice versa.

Theoretical considerations show that the average grain size of the product phase is given approximately by the so-called *Avrami length*, either in 3D (δ_{Av}, grain size after completion of the transformation), or in 2D (δ_{Av}^{2D}, grain diameter at the formation of continuous films), whereas the half-time of both processes is of the order of the so-called *Avrami time* (τ_{Av} or τ_{Av}^{2D}). These scaling parameters are defined by (see [6]):

$$\delta_{Av} = \left[I^V / Y \right]^{-1/4}, \quad \delta_{Av}^{2D} = \left[I^B / Y \right]^{-1/3} \tag{6}$$

and:

$$\tau_{Av} = \left[I^V Y^3 \right]^{-1/4}, \quad \tau_{Av}^{2D} = \left[I^B Y^2 \right]^{-1/3} \tag{7}$$

for constant nucleation and growth rates. Here, I^V is the nucleation rate per unit volume; that is, the product of the grain-boundary nucleation rate, I^B, and the grain-boundary area per unit volume of the reactant phase ${}^{\upsilon}O^B$:

$$I^V = I^B {}^{\upsilon}O^B \tag{8}$$

More generally, for time-dependent P–T conditions, Eqs. (6) and (7), calculated at 1% and 99% transition degree, define the range of change of average grain size and transition half-time during the transformation [6]. We shall utilize both scaling laws here: (1) to infer the spinel grain size at or near the formation of continuous films of spinel phase along the olivine grain boundaries (''spinel percolation'') on the basis of Eq. (6), and (2) to estimate the amount of metastable overshoot on the basis of Eq. (7).

In order to estimate the creep strength of a slab during its subduction, we need to know the spinel grain size at a given point in space, $\delta_{sp}(x, z)$. For this purpose, we calculate the expected spinel grain size at the beginning of the phase transformation (1st kinetic phase boundary at $\xi = 1\%$) assuming that it is given by the local value of the Avrami length, Eq. (6). Afterwards, the spinel grain size changes by two main processes: (1) crystal growth of newly formed spinel grains at the expense of the olivine host phase; and (2) competitive growth of neighbouring ''old'' spinel grains. In the following, we will make the assumption that the spinel contribution to the composite slab strength in the two-phase region is given by those spinel grains that first formed the continuous films at the beginning of the transformation (process 1). This seems to be justified for cold slabs with a potentially large grain-size reduction, since the dramatic drop in creep strength associated with this reduction would lead to a large viscosity contrast between the stiff matrix of predominantly olivine grains and the weak continuous spinel films percolating through this matrix. The location of this percolation transition is dependent on the extent of grain-size reduction and is therefore kinetically defined. Typically, for a grain-size reduction of 10–100, the percolation transition happens at 10–1% degree of transition [6].Competitive grain growth of fine-grained spinel after site saturation and complete impingement along the olivine grain boundaries (process 2) is likely to occur according to:

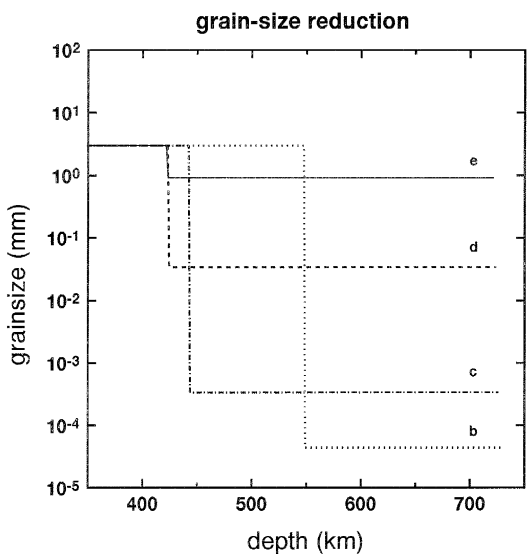

Fig. 3. Grain-size reduction accompanying the olivine → spinel transformation and subsequent grain growth in the coldest portion of downgoing slabs. The P–T paths and the labelling as in Fig. 2. Spinel grain growth (not included in the model) would increase again the grain size at greater depth depending on the P–T conditions.

$$\delta_{sp}(t)^n - \delta_0^n = k_0 \int_0^t \exp\left[-\frac{E_* + PV_*}{RT}\right] dt' \tag{9}$$

where E_* and V_* are activation energy and activation volume for spinel grain growth, respectively, and δ_0 is the grain size at $\xi = 1\%$ given by Eq. (6).

Since there are no detailed experimental data available on the grain-growth kinetics in β- or γ-spinel of Mg_2SiO_4, we refrain here from a quantitative modelling of this process. Qualitatively, it is intuitively clear that — according to Eq. (9) — spinel grain growth will be very sensitive to slab temperature, and small grain size will last only to greater depth when temperatures are low; for example, in the interior of fast subducting slabs.

Within the framework of the present model, the grain size of newly formed spinel will become very large when transformation and subsequent grain growth occur at high temperatures. These very large spinel grain sizes are not realistic, since the growing spinel grains will collide with other minerals, such as pyroxenes or garnets, when the size of newly formed grains exceeds the average size of the starting mate-

rials ($\sim$ 3 mm; see, e.g., [25]). At this point growth will stop and the present model will not work. Therefore, in the following we set an upper limit of 3 mm for the spinel grain size.

The resulting grain-size development of spinel with depth for the different P–T paths of Fig. 2 is plotted in Fig. 3. As it can be seen, a grain-size reduction of up to 4–5 orders of magnitude is possible for slab temperatures below 900 K. The physical reason for this dramatic drop in grain size is the large metastable overshoot, $\Delta\mu$, present at these low temperatures, which leads to a significant change in the balance between nucleation and growth, see discussion.

4. Rheological structure of subducted slabs

The rheology of olivine is now reasonably well understood, including the effects of temperature, stress and grain size, although some critical issues, such as the effects of pressure and water, still need further investigation (for a review, see [26,27]). In contrast, the rheology of spinel or modified spinel is very poorly constrained. The only experimental data on spinel rheology is that of Vaughan and Coe [1] and Tingle et al. [28] on a germanate analogue. Some preliminary observations are also available for modified spinel [29,30] suggesting higher strength of modified spinel than olivine in the dislocation creep regime (see also [3]). In the absence of direct experimental data on the rheology of $(Mg, Fe)_2SiO_4$ spinel or modified spinel, we take the admittedly crude approximation that the rheology of spinel or modified spinel is the same as that of the spinel phase of the germanate analogue (Mg_2GeO_4), after the normalization of temperature by the melting temperature (T/T_m) and stress by the shear modulus (σ/μ).

Considering the strength distribution of oceanic lithosphere at upper mantle P–T conditions, slab deformation is mainly controlled by olivine creep [31,32]. For differential stresses (σ) below 200 MPa the dominant mode of deformation is power-law creep:

$$\frac{\mathrm{d}\epsilon}{\mathrm{d}t} = C_1\sigma^3\exp\left[-\frac{Q_1 + PV_1}{RT}\right] \tag{10}$$

where: $\mathrm{d}\epsilon/\mathrm{d}t$ is the creep rate; R is the gas constant; Q_1 is the creep activation energy; V_1 is the creep activation volume; and C_1 is a constant. For differential stresses greater than 200 MPa (low-temperature plasticity), the relevant deformation mechanism is glide-controlled creep (Peierls stress controlled dislocation glide, σ_p):

$$\frac{\mathrm{d}\epsilon}{\mathrm{d}t} = C_2\exp\left[-\frac{Q_2}{RT}\left(1-\frac{\sigma}{\sigma_p}\right)^2\right] \tag{11}$$

with $\sigma_p = 8.5$ GPa ([32]), the activation energy Q_2, and a constant C_2.

During fast subduction, any deformation of the cold slab interior is probably described by Eq. (11), where the values of Q_2 and σ_p have to be modified to account for the effect of pressure. One possibility to include depth- or pressure-dependence into the creep laws is by rescaling the appropriate activation energies with the depth- or pressure-dependent melting temperature of the material (mantle solidus). We adopt here the method of Rubie [2] and rescale the corresponding parameters according to:

$$Q_2' = Q_2 \cdot \frac{\mu b^3}{\mu_0 b_0^3} \text{ and } \sigma_p' = \sigma_p \cdot \frac{\mu}{\mu_0} \tag{12}$$

where μ and b are the shear modulus and Burgers vector, respectively, at pressure p, and μ_0 and b_0 are the same parameters at 1 atm. The creep law of fine-grained spinel with grain size δ_{sp} is estimated using the experimental data on Mg_2GeO_4 spinel [1] according to:

$$\frac{\mathrm{d}\epsilon}{\mathrm{d}t} = C_{m,n}\delta_{sp}^{-m}\sigma^n\exp\left[-\frac{Q_{sp} + PV_{sp}}{RT}\right] \tag{13}$$

Here, Q_{sp} and V_{sp} are the activation energy and activation volume for spinel creep, and $C_{m,n}$ are suitable constants. We note that this rheological constitutive relation for spinel is not well constrained. For example, for oxide spinel, the dominant deformation mechanism at small grain size is linear diffusion creep rather than non-linear ''superplasticity'' [33]. Because of this uncertainty, we use three alternative creep laws to model the rheology of spinel: (1) Nabarro–Herring diffusion creep, assuming that diffusion occurs through the lattice ($m = 2,\ n = 1$);

(2) Coble diffusion creep, assuming that diffusion occurs predominantly along grain boundaries ($m = 3$, $n = 1$); and (3) structural superplasticity, assuming that grain-boundary sliding is accommodated not by diffusion but by climb of dislocations at grain boundaries ($m = 2$, $n = 2$) [34]. The values of the respective constants $C_{m,n}$ are chosen to fit Eq. (13) with the experimental data by Vaughan and Coe [1], a method similarly employed in [2].

When the grain-size reduction is not large, then other deformation mechanisms such as the Peierls mechanisms or power-law creep will dominate. The creep strength in these mechanisms is not very different between olivine and spinel [3,28] and we assume that they are identical in this paper. Estimated rheological parameters for olivine and spinel are summarized in Table 2.

In the two-phase region, we calculate the rheological properties of mixed aggregates of olivine and spinel on the basis of phenomenological flow laws for composite viscous materials. According to this approach [9], the composite creep strength is either given by:

$$\sigma_{\text{two-phase}} = (1 - \xi) \cdot \sigma_{\text{ol}} + \xi \cdot \sigma_{\text{sp}} \tag{14}$$

for no grain-size reduction (when spinel forms a ''load-bearing framework'' within the olivine matrix), or by:

$$\sigma_{\text{two-phase}} = \left(1 - \xi^{(\sigma_{\text{sp}}/\sigma_{\text{ol}})}\right) \cdot \sigma_{\text{ol}} + \xi^{(\sigma_{\text{sp}}/\sigma_{\text{ol}})} \cdot \sigma_{\text{sp}} \tag{15}$$

for grain-size reduction during transformation (spinel grains form a ''interconnected weak layer'' structure, a type of microstructure similar to the one studied theoretically in [6]). Here, ξ is the volume fraction of spinel, and σ_{ol} and σ_{sp} are the respective creep strengths of the end-member minerals. Eq. (15) has been suggested to describe the composite flow strength of quartz mylonite in quartz–feldspar granitic rock [9], where quartz forms an interconnected matrix of dynamically recrystallized grains that envelop rounded feldspar grains. The deformation stress and strain has been found to be largely partitioned into the fine-grained quartz matrix, whereas, in contrast to quartz, the feldspar grains show few traces of internal strain ([9], p. 290). Here, we argue that a similar situation could arise in the case of a large grain-size reduction resulting from the olivine–spinel phase transformation, so that most of the strain of the slab is partitioned into the relatively weak spinel phase surrounding the olivine host grains.

Table 2
Rheological parameters for olivine and spinel

Parameter	Value
Pre-exponential constant C_1, Eq. (10) [31]	7.0×10^{-14} s^{-1} Pa^{-3}
Activation energy for power-law creep, Q_1, Eq. (10) [32]	523 kJ mol^{-1}
Activation volume for power-law creep, V_1, Eq. (10) [45]	1.4×10^{-5} m^3 mol^{-1}
Pre-exponential constant, C_2, Eq. (11) [31]	5.7×10^{11} s^{-1}
Activation energy for Peierls stress creep, Q_2, Eq. (11) [31]	536 kJ mol^{-1}
Peierls stress for olivine, σ_p, Eq. (11) [31]	8.5 GPa
Burgers vector of olivine at 1 atm and 300 K b_0, Eq. (12) [32]	6.0×10^{-10} m
Bulk modulus of olivine at 1 atm and 300 K [32]	127 GPa
Shear modulus of olivine at 1 atm and 300 K μ_0, Eq. (12) [32]	81.3 GPa
Pressure dependence of shear modulus, $\mathrm{d}\mu/\mathrm{d}p$ [32]	1.8
Constant C_{21}, Eq. (13) (Nabarro–Herring creep)	2.34×10^{-14} s^{-1} m^2 Pa^{-1}
Constant C_{31}, Eq. (13) (Coble creep)	7.02×10^{-20} s^{-1} m^3 Pa^{-1}
Constant C_{22}, Eq. (13) (superplasticity)	2.34×10^{-23} s^{-1} m^2 Pa^{-2}
Activation energy for spinel creep, Q_{sp}, Eq. (13) [1]	296 kJ mol^{-1}
Activation volume for spinel creep, V_{sp}, Eq. (13) [1]	5.33×10^{-6} m^3 mol^{-1}

According to Eq. (15), a significant reduction in composite flow strength is possible with only a few percent of spinel phase, provided that the contrast in creep strength between both phases is large enough ($\sigma_{sp} \ll \sigma_{ol}$).

5. Results and discussion

The most significant result of this paper is the demonstration that a large grain-size reduction can be associated with the olivine to spinel transformation when the transformation occurs at relatively low temperatures but not at high temperatures. The degree of grain-size reduction predicted by the present model for relatively cold slabs ($T \leq 900$ K) is very large (down to less than 1 μm) and one expects a significant reduction in creep strength in these cases. Before we discuss potential implications, it is appropriate to interpret our results and compare them with some laboratory observations.

The numerically calculated spinel grain sizes δ_0 at $\xi = 1\%$ (near the percolation threshold) are plotted as a function of temperature in Fig. 4. The results include slabs with different initial temperature distributions (variable thicknesses) and different subduction velocities. They show that the dependence of spinel grain size on slab temperature consists of two different branches, in close relationship to the existence of two branches of the kinetic phase boundary shown in Fig. 2. At high temperatures (branch A), spinel grain size depends on temperature as $\delta_0 \sim \exp(-E^*/RT)$, whereas in cold portions of slabs (branch B), a more complicated behaviour is found:

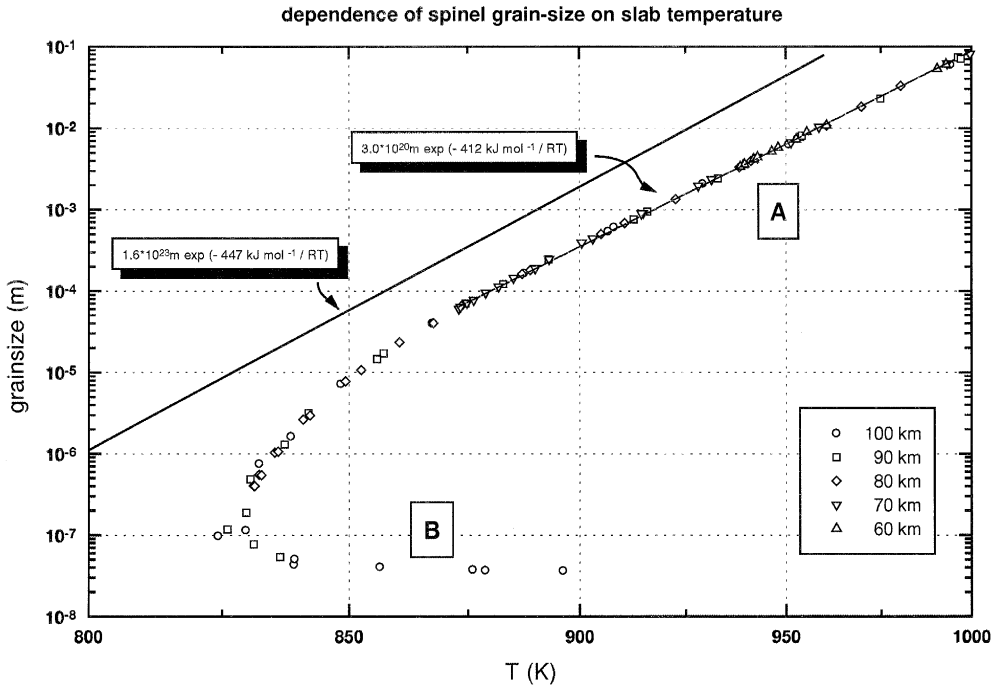

Fig. 4. Arrhenius plot of spinel grain size (logarithmic scale) vs. temperature (reciprocal scale), both numerically determined at the first kinetic phase boundary ($\xi = 1\%$) for different slab thicknesses. The symbols show the values obtained of spinel grain size at $\xi = 1\%$ for different subducting layers of lithosphere across the slab. Above 900 K, they follow an Arrhenius dependence with an apparent ''activation energy'' of about 412 kJ/mol (branch A). Shown as a thick solid line is the semi-analytical solution of Eq. (A6), predicting a slightly higher value of 447 kJ/mol. Note that, within the metastable wedge, the apparent ''activation energy'' for spinel grain size can be negative (branch B). Predicted grain sizes exceeding ~ 3 mm are not realistic since the presence of secondary phases such as pyroxenes and garnets prevents the formation of larger spinel grains.

At lower temperatures, the logarithmic plot of grain size vs. T has a negative slope; that is, grain size can decrease with temperature in a certain range.

To interpret this observation and to compare the results with laboratory experiments, we rewrite Eq. (6) as:

$$\delta_0 \sim Y \cdot \tau_{\mathrm{Av}} \tag{16}$$

Now, within the high temperature branch of the kinetic phase boundary (branch A), the transformation occurs near to equilibrium and the distance between kinetic and equilibrium phase boundary depends only weakly on temperature. The main effect of temperature on grain size comes from the growth rate term (Y) and hence:

$$\delta_0 \sim \exp\left[-\frac{Q_a + PV_a}{RT}\right] \tag{17}$$

Eq. (17) has an Arrhenius type temperature dependence with an apparent ''activation energy'' similar to that of growth kinetics, in accordance with the numerical results shown in Fig. 4.

Within the low temperature branch (branch B), the transformation occurs only at a significant overstepping over equilibrium. The amount of metastable overshoot, ΔP, necessary to start the transformation kinetics can be estimated on the basis of a time scale argument [6,35]: The transformation time scale, τ_{Av}, must be of the order of the time required to pass the overshoot:

$$\tau_{\mathrm{Av}}(\Delta P{-}T) \cong \frac{\Delta P}{\rho g v_{\mathrm{slab}}} \tag{18}$$

Together with the nucleation and growth rates according to Eq. (2) and Eq. (3), Eq. (18) defines an implicit relationship for the kinetic phase boundary $P_{\mathrm{kin}}(T)$ ($\Delta P \equiv$ metastable overshoot, $P_{\mathrm{kin}} - P_{\mathrm{eq}}$) in dependence of temperature, T, which can be solved numerically (a detailed analysis is given in Appendix A).

We find the solution obtained, $\Delta P(T)$, on the basis of Eq. (18) in good agreement with the numerical result of the Runge–Kutta integration of the kinetic differential equations, where we calculate $\Delta P(T)$ under the assumption that P_{kin} is given by the pressure value at 1% transition degree. Both calculation schemes show that metastable hindrance can cause an overshoot of up to 200 km and more at temperatures below 850 K, see Fig. 5. Typically, ΔP ranges between 0.7 and 0.4 GPa at temperatures between 950 and 1300 K. Below 900 K, the persistence of metastable olivine to greater depth leads to a different T dependence. Analytically, it follows from Eq. (6) at $\Delta\mu \gg RT$:

$$\delta_0 \cong \left[I_0^B/Y_0\right]^{-1/3} \exp\left[+\frac{c_1}{T(\Delta\mu)^2}\right] \tag{19}$$

with $c_1 = 16\pi\eta\sigma^3 V_m^2/9k$, and $\Delta\mu(T)$ is an almost linearly increasing function of T (see Appendix A). Eq. (19) predicts a minimum grain size of $\delta_0 \sim (I_0^B/Y_0)^{-1/3}$ at very large overshoots, whereas at intermediate $\Delta\mu \geq RT$, it predicts a grain size decrease with increasing temperature (branch B of Fig. 4).

The present results may also be compared with some experimental observations. Rubie and Brearley [36] and Brearley et al. [37] transformed hot pressed forsterite powder to its high-pressure polymorphs by gradually increasing the pressure into the spinel stability field ($P = 15$ GPa) at nearly constant temperatures ($T = 1173$ K) at the laboratory time scale (duration of the experiments 1 h and 5 h, respectively). Their experimental data on grain size of modified spinel phase should therefore be comparable with the here presented grain-size estimations based on the Avrami length taken at these P–T conditions. The results are shown in Fig. 5 and Table 3. There appears to be a reasonable agreement between the experimental observations and the theoretical estimations, both as to the reachable P–T conditions at the laboratory time-scale as well as to the reported spinel grain sizes. The large difference between laboratory and geologic time scale results hereby in large grain-size differences at the same reference temperature (according to Eq. (A9)), but these differences are, to a great extent, compensated again by the entirely different temperature conditions.

We point out here, however, that the grain-size estimations presented are largely based on the current understanding of the transformation process from olivine to spinel under subduction zone conditions (as reviewed, e.g., in [38,24]). More recent work of Kerschhofer et al. [39] shows that intracrystalline nucleation of spinel may become important at large

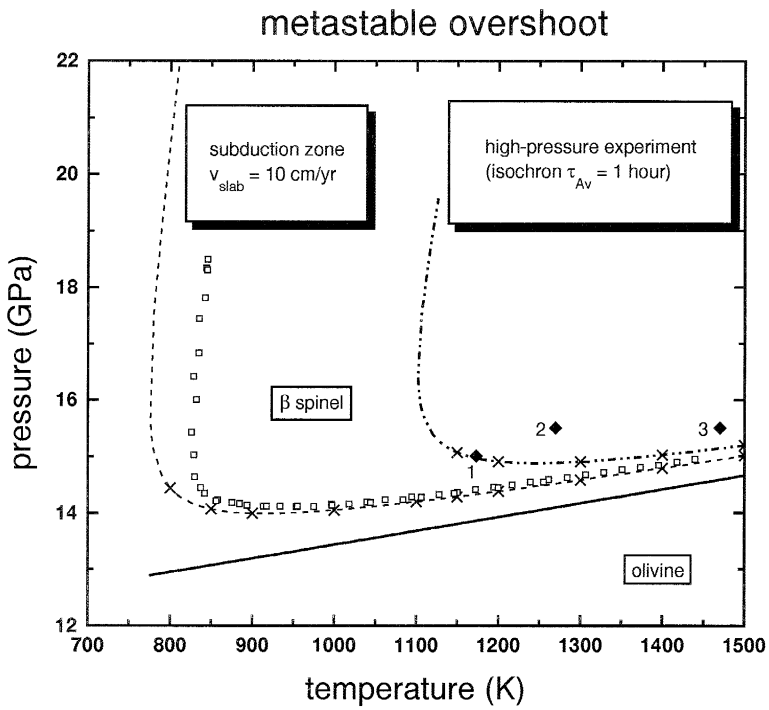

Fig. 5. Calculated metastable overshoot $\Delta P = P_{kin} - P_{eq}$ of olivine over the equilibrium pressure with β-Mg_2SiO_4 (Eq. (A6)) under subduction zone conditions (dashed line). The squares show the numerically calculated onset of transformation at $\xi = 1\%$ for a slab with thickness $L = 100$ km (integration of the differential Eqs. (A4) and (A5), thick line = phase equilibrium). For comparison, the isochron $\tau_{Av} = 1$ h is included, showing the expected location of the kinetic phase boundary at the laboratory time scale (dash-dotted curve). At the geological time-scale, wedge formation sets in at temperatures below 850 K. A compilation of some spinel grain sizes at selected P–T conditions (crosses) is given in Table 3; solid diamonds mark the reported P–T conditions of three different high pressure experiments: (1) $P = 15$ GPa, $T = 1173$ K [36], spinel grain size $\cong 1$ μm, Eq. (6) predicts 1.8 μm; (2) $P = 15.5$ GPa, $T = 1273$ K [16], spinel grain size $\cong 1.8$ μm, Eq. (6) predicts 0.4 μm, (3) $P = 15.5$ GPa, $T = 1473$ K [46], spinel grain size not mentioned, Eq. (6) predicts 4.6 μm.

Table 3
Spinel grain size: comparison with laboratory data

T	Subducting slab ($v_{slab} = 10$ cm/yr)				Experimental ($\tau_{Av} = 1$ h)		
(K)	ΔP (GPa)	P_{kin} (GPa)	δ_0 (m)	Eq. (A9) (m)	ΔP (GPa)	P_{kin} (GPa)	δ_0 (m)
1500	0.35	15.00	$4.61 \cdot 10^{7}$	$4.87 \cdot 10^{7}$	0.54	15.19	$6.70 \cdot 10^{-2}$
1400	0.37	14.79	$3.56 \cdot 10^{6}$	$3.64 \cdot 10^{6}$	0.61	15.02	$4.90 \cdot 10^{-3}$
1300	0.41	14.58	$1.84 \cdot 10^{5}$	$1.97 \cdot 10^{5}$	0.73	14.90	$2.39 \cdot 10^{-4}$
1200	0.45	14.38	$5.83 \cdot 10^{3}$	$6.19 \cdot 10^{3}$	0.98	14.90	$6.90 \cdot 10^{-6}$
1150	0.48	14.28	$8.27 \cdot 10^{2}$	$8.96 \cdot 10^{2}$	1.26	15.06	$8.99 \cdot 10^{-7}$
1100	0.51	14.19	$9.84 \cdot 10^{1}$	$1.06 \cdot 10^{2}$	not reachable in high-pressure experiments		
1000	0.61	14.05	$7.38 \cdot 10^{-1}$	$8.22 \cdot 10^{-1}$			
900	0.80	13.99	$1.91 \cdot 10^{-3}$	$2.25 \cdot 10^{-3}$			
850	0.99	14.07	$5.80 \cdot 10^{-5}$	$7.10 \cdot 10^{-5}$			
800	1.49	14.44	$1.12 \cdot 10^{-6}$	$1.56 \cdot 10^{-6}$			

Predicted spinel grain size, δ_0, on the basis of Eq. (6), numerically calculated at the first kinetic phase boundary defined by Eq. (A6). For comparison, we show in the right panel the predicted spinel grain size for a high-pressure experiment at the laboratory time scale ($\tau_{Av} =$ 1 h). The data points are shown as crosses in Fig. 5.

metastable overshoots of about 18–20 GPa and relatively low temperatures of 1000–1400°C. As of now, since these newly found results are not quantified yet, we state only that an additional shear-induced coherent nucleation mechanism would, of course, affect the above grain size estimations, and that these new findings could be of particular importance for the overall transition kinetics; possible effects could be either a considerable narrowing of the depth of the region of olivine–spinel coexistence or a reduction in the metastable overshoot of olivine in cold slabs.

The strong dependence of spinel grain size on temperature under the P–T conditions of subducting slabs gives rise to the surprising possibility that the effective viscosity of the slab after the olivine–spinel phase transformation could be higher at higher temperatures (see also the discussion by Rubie and Ross [10], p. 238). In order to investigate this possibility more quantitatively, we plot the creep strength within the slab for a representative strain rate of 10^{-15} s^{-1} on the basis of appropriate constitutive equations for olivine and spinel creep in Figs. 6 and 7.

Fig. 6 shows the creep strength of the slab vs. depth along the coldest portion for three different spinel creep laws and two different subduction velocities. As can be seen, the creep strength in the central portions of fast slabs drops down by several orders of magnitude and assumes a minimum near to the depth where the phase transformation is almost completed (2nd kinetic phase boundary, $\xi = 99\%$). This behaviour appears to be typical for all three grain-size sensitive creep laws (Nabarro–Herring creep, Coble creep and superplasticity, compare Table 2). In contrast, the creep strength of a slow slab remains well above these values, suggesting that a warm slab could be (partially) stronger than a cold slab.

In Fig. 7, we extend this figure into a two-dimensional plot in order to show the rheological structure of a whole slab (Nabarro–Herring creep only). As expected from Fig. 6, a localized weak zone develops below the tip of the metastable olivine wedge. This weak zone can occupy up to 20% of the slab interior, thus dividing the slab into two comparatively stronger layers at the top and bottom, at depths between 450 and 600 km. In this way it is acting as a kind of low pressure inclusion within the slab body, since the stronger bottom and top layers prevent the

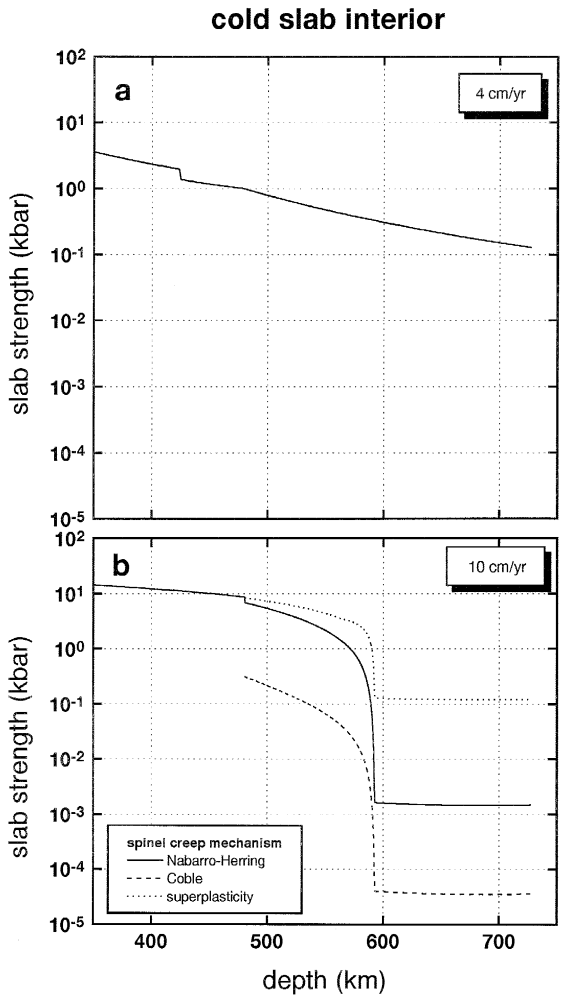

Fig. 6. Creep strength of the slab shown in Fig. 1 along its coldest part (slab thickness 85 km) below 400 km. The grain size reduction produces a strength drop of several orders in magnitude, in dependence of the relevant spinel creep mechanism. An average strain rate of 10^{-15} s^{-1} is assumed uniformly across the slab.

undelayed accommodation of the associated density increase by the surrounding hotter mantle. The likely existence of complex internal states of stress produced by the effects of the volume changes accompanying the transformation of peridotite to the transition zone mineral assemblage has also been emphasized recently by Kirby and Okal [40].

Finally, we comment briefly on some geodynamic implications of the present study. It has been argued that deep earthquake activities are related to the

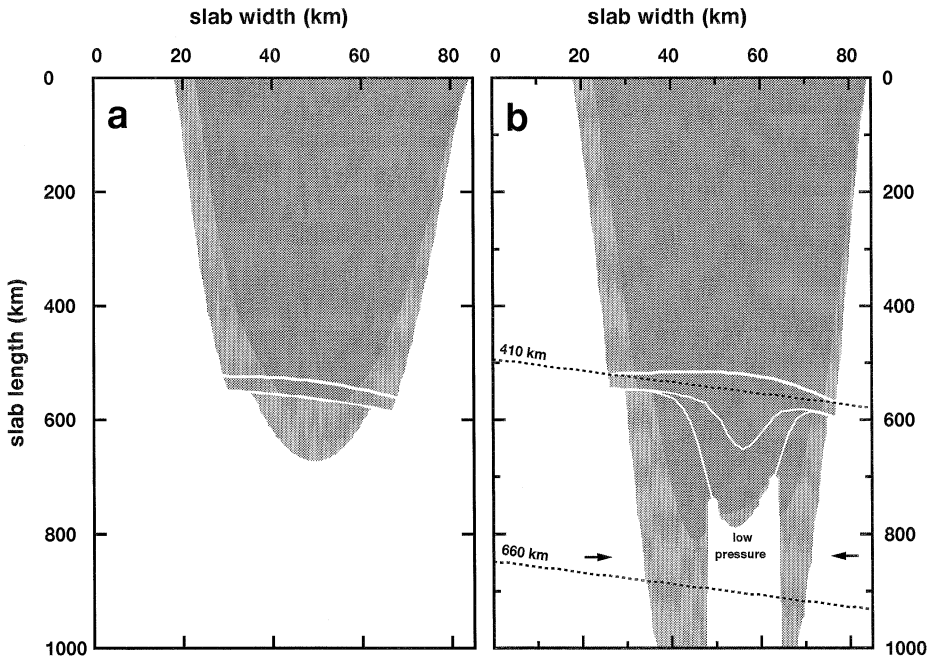

Fig. 7. Calculated strength profile of the slab shown in Fig. 1 on the basis of a Nabarro–Herring creep mechanism for spinel (m = 2 and n = 1 in Eq. (13)). The creep strength of spinel is assumed to be bounded by the olivine creep strength within the slab. The grey area shows the slab portions with a creep strength higher than 100 MPa; the dark grey shows the slab portions with a creep strength higher than 200 MPa. Note the dramatic strength drop below the tip of the metastable wedge. Spinel grain growth (not included in the model) would cause a significant decrease in the size of the weak zone below the metastable wedge. The two arrows indicate the possible effect of a sustainable pressure drop in the cold interior of fast slabs (see discussion).

transformation of metastable olivine to the modified or spinel phase, since seismicity is high in slabs where metastable olivine is considered to occur [5,38,24,41,42]. Deep earthquakes are hereby believed to occur as a result of the instability of deformation in the ductile regime. The present results provide some insight into the possible mechanisms of deep earthquakes. Combined with the results of thermal models of slabs [19], we propose that the nature of instabilities associated with the olivine–spinel transformation is fundamentally different between the cold and warm branches of the kinetic phase boundary and that instabilities will occur only when the transformation occurs in the cold branch. Our studies suggest two instability mechanisms. One is thermal runaway due to the latent heat release [19]. We have shown that the latent heat release causes positive feedback only when the transformation occurs in the cold branch but not in the hot branch [19], compare also Fig. 2.

Similarly, the effects of grain-size reduction to cause softening and hence instability will be important only in the cold branch because significant grain-size reduction occurs only at relatively low temperatures. In addition, since the degree of grain-size reduction increases with temperature in this regime (see Fig. 4 and Eq. (19)), a self-accelerating instability is prone to occur there. Thus, both the effects of latent heat and of grain-size reduction tend to lead to shear instability in the cold branch but not in the hot branch.

6. Conclusions

Our theoretical calculations have shown that the olivine–spinel transformation in subducting slabs can indeed result in a significant grain-size reduction and resultant rheological weakening. We have also shown that the effect is highly sensitive to temperature at

which the phase transformation occurs. These predictions are consistent with experimental observations that the size of grains formed by nucleation and growth tends to be small when transformation occurs at relatively low temperatures.

The present results, however, have some limitations which have to be further investigated in future studies. First, some parameters in transformation kinetics are not well constrained. In particular, parameters related to nucleation processes are poorly constrained [10,39]. This leads to large uncertainties in grain size in the low temperature regime (see Eq. (19)), although it will not affect the results in the high temperature regime (Eq. (17)). In addition, changes in the nucleation and growth rates due to the accompanying pressure drop are neglected. Second, the flow laws for spinel in the grain-size sensitive regime are poorly constrained, which leads to large uncertainties in estimated strength from grain size and temperature (and pressure), Figs. 6 and 7. Third, the temperatures in slabs are also only poorly constrained, the main uncertainties include the effects of shear heating and of latent heat. Thus, the details of the present results must be taken with caution. However, the notion of large rheological weakening due to grain-size reduction in cold slabs seems robust and should be taken into account in any models of slab dynamics.

Acknowledgements

We thank Dave Rubie and Slava Solomatov for critical reviews. We thank Ramesh Kizhappali for discussion. This research was supported by the Deutsche Forschungsgemeinschaft and the National Science Foundation, grant EAR-9505451 (to S.K.). ***[UC]***

Appendix A

A.1. Kinetics of grain-boundary nucleated reactions

We give here a brief derivation of the kinetic equations used in the modelling section. The overall tranformation rate, $\xi(t)$, under constant P–T conditions for grain boundary nucleated reactions was derived by Cahn [20] as:

$$\xi(t) = 1 - \exp\left\{ -2\,{}^{v}O^{B} \int_0^t \left[1 - \exp(-A_e)\right] Y \mathrm{d}t' \right\} \tag{A1}$$

where ${}^{v}O^{B}$ is the grain boundary area per unit volume of the host phase; Y is the (constant) growth rate of new phase grains; and A_e is the increase in the extended area fraction of new phase material owing to all the grains nucleating at a time between t' and t. Eq. (A1) has been generalized to non-isothermal, non-isobaric transformations by Rubie and Ross [10]. For this more general case, A_e is given by:

$$A_e(t,t') = \pi \int_0^{t-t'} I^{B}(\tau) \left[\left(\int_\tau^t Y(t'')\mathrm{d}t'' \right)^2 - \left(\int_\tau^{t'} Y(t'')\mathrm{d}t'' \right)^2 \right] \mathrm{d}\tau \tag{A2}$$

with $I^{B}(\tau)$ as the grain boundary nucleation rate of spinel, and Eq. (A1) is generalized to:

$$\xi(t) = 1 - \exp\left\{ -2\,{}^{v}O^{B} \int_0^t \left[1 - \exp(-A_e(t,t'))\right] \times Y(t')\mathrm{d}t' \right\} \tag{A3}$$

The numerical solution of Eq. (A2) and Eq. (A3) is rather difficult and possible only by employing a time-consuming iterative integration procedure for each time step (see appendix in [10] for details). Hence, it seems to be impossible to apply them to the whole transforming slab within reasonable cpu times. Furthermore, the necessary iteration steps are a possible source of numerical errors.

Here, we simplify the kinetic analysis on the basis of the following observation: At starting transformation (undersaturated nucleation), the overall transition kinetics are indistinguishable from a homogeneous nucleation and growth process. This can be shown to be valid as long as the kinetically determined Avrami length δ_{Av} is larger or in the same order as the initial grain size of the host phase,

$L_{\mathrm{ini}} \sim 1/{}^{v}O^{B}$ [6]. At later stages, site saturation along the preferred nucleation sites at grain boundaries sets in and leads to linear growth of new phase grains at the already transformed grain boundaries. It has been shown [20], that this change (site saturation and change from $3D \rightarrow 1D$ growth) occurs in a rather narrow time interval during the transformation, in the vicinity of the percolation point ξ_{Per} of the new phase grains. As a consequence, it is possible to solve the two limiting cases separatedly instead of Eqs. (A2) and (A3), and to switch between both cases numerically, depending on the calculated transformed volume degree $\xi(t) = 1 - \exp(-X_{3D}(t))$; X_{3D}, X_{2D}, X_{1D}, and X_{0D} denote in the following the total grain volume, grain area, grain diameter, and grain number of the product phase (as defined in [6], p. 398).

Case (1): Homogeneous nucleation, $\xi(t) \leq \xi_{\mathrm{Per}}(\exp[-A_e] \approx 1 - A_e)$:

$$\frac{\mathrm{d}}{\mathrm{d}t}X_{3\mathrm{D}}(t) = 4 \cdot Y(t) \cdot X_{2\mathrm{D}}(t)$$

$$\frac{\mathrm{d}}{\mathrm{d}t}X_{2\mathrm{D}}(t) = \pi \cdot Y(t) \cdot X_{1\mathrm{D}}(t)$$

$$\frac{\mathrm{d}}{\mathrm{d}t}X_{1\mathrm{D}}(t) = 2 \cdot Y(t) \cdot X_{0\mathrm{D}}(t)$$

$$\frac{\mathrm{d}}{\mathrm{d}t}X_{0\mathrm{D}}(t) = I^{V}(t) \qquad \text{(A4)}$$

with $I^{V}(t) = {}^{v}O^{B}\ I^{B}(t)$, and:

Case (2): Site-saturated nucleation, $\xi(t) \geq \xi_{\mathrm{Per}}$ $(\exp[-A_e] \approx 0)$:

$$\frac{\mathrm{d}}{\mathrm{d}t}X_{3\mathrm{D}}(t) = 2 \cdot Y(t)\,{}^{v}O^{B} \qquad \text{(A5)}$$

The percolation threshold for grain boundary nucleated reactions, ξ_{Per}, is dependent on the $L_{\mathrm{ini}}/\delta_{\mathrm{Av}}$ ratio of the host phase and is calculated on the basis of the numerical simulation algorithm described in [6]. For a grain-size reduction of several orders in magnitude (i.e., $\delta_{\mathrm{Av}} \ll L_{\mathrm{ini}}$) it is well below $\xi \sim 1\%$, and Eq. (A5) applies almost everywhere in the two-phase region of the slab.

A.2. kinetic phase boundary

The metastable overshoot, ΔP, follows from Eq. (18), combined with Eqs. (2) and (3) and Eq. (7). After insertion, one obtains the following transcendental equation for $\Delta P(T)$:

$$\ln\left[\frac{\Delta P T}{A_0}\right] = \frac{A_1}{T} + A_1' + \frac{A_1'' \Delta P}{T} + \frac{A_2}{T(\Delta P)^2} - \frac{2}{3}\ln\left[1 - \exp\left(-\frac{A_3 \Delta P}{T}\right)\right] \qquad \text{(A6)}$$

with the constants $A_0 = \rho g v_{\mathrm{slab}} / \sqrt[3]{I_0^B Y_0^2}$, $A_1 = (Q_a + P_0 V_a)/R$, $A_1' = \Delta S V_a / \Delta V R$, $A_1'' = V_a/R$, $A_2 = 16\pi\eta\sigma^3 V_m^2 / 9k(\Delta V)^2$, and $A_3 = \Delta V/R$.

Eq. (A6) is numerically solved with a Newton–Raphson iteration algorithm. It has a single solution for $A_1'' = 0$; that is, for vanishing pressure effect on the activation energy. At finite A_1'', a second solution appears for overcritical overpressures $\Delta P > \Delta P_{\mathrm{crit}}$. The critical overpressure ΔP_{crit}, where the kinetic phase boundary bifurcates in two branches $(d\Delta P/dT \rightarrow -\ )$, is approximately given with:

$$(\Delta P_{\mathrm{crit}})^3 \approx \frac{2A_2}{A_1''} = \frac{32\pi\eta\sigma^3 N_A V_m^2}{9V_a(\Delta V)^2} \qquad \text{(A7)}$$

where N_A is Avogadro's number. At small $\Delta\mu \ll RT$, we find:

$$\Delta P(T) \cong \frac{V_m}{\Delta V} \times \left(\frac{16\pi\eta\sigma^3/9kT}{\ln\left(T\sqrt[3]{I_0^B Y_0^2}\,\Delta P/\rho g v_{\mathrm{slab}}\right) - (Q_a + P_{\mathrm{eq}}V_a)/RT}\right)^{1/2} \qquad \text{(A8)}$$

to logarithmic accuracy.

The expected spinel grain size at $\Delta\mu \ll RT$ is given with (Eq. (17)):

$$\delta_0 \cong \frac{Y_0 \Delta V (\Delta P)^2}{\rho g v_{\mathrm{slab}} R} \exp\left[-\frac{Q_a + P_{\mathrm{kin}}V_a}{RT}\right] \qquad \text{(A9)}$$

Eq. (A9) is an Arrhenius relationship with an apparent activation energy, Q_{gs}, close to the activation energy for diffusion of atomic units to the

growing interface, Q_a. Neglecting the weak dependence of ΔP on T, Q_{gs} has the order of magnitude:

$$Q_{\mathrm{gs}} \sim Q_a + P_0 \cdot V_a \sim 467\ \mathrm{kJ/mol} \qquad \text{(A10)}$$

where P_0 is the (extrapolated) intercept of the Clausius–Clapeyron equation with the pressure axis at $T = 0$ K. In contrast, at large $\Delta\mu \gg RT$, we obtain (Eq. (19)):

$$\delta_0 \cong \left[I_0^B / Y_0 \right]^{-1/3} \exp\left[+ \frac{16\pi\eta\sigma^3 V_m^2}{9kT(\Delta\mu)^2} \right] \qquad \text{(A11)}$$

with:

$$\Delta\mu(T) = \frac{\Delta V}{V_a} \left\{ RT \ln\left[\frac{T\sqrt[3]{I^{B_0} Y_0^2}\,\Delta P}{\rho g v_{\mathrm{slab}}} \right] - \left(Q_a + P_{\mathrm{eq}} V_a \right) \right\} \qquad \text{(A12)}$$

The critical depth that separates both cases Eqs. (A9) and (A11) can be found from the condition $\Delta\mu \sim RT$. This depth is for the olivine–spinel transformation at 850 K given by:

$$\Delta z \cong \frac{RT}{\rho g \Delta V} \sim 69\ \mathrm{km} \qquad \text{(A13)}$$

References

[1] P.J. Vaughan and R.S. Coe, Creep mechanism in Mg_2GeO_4: Effects of a phase transition, J. Geophys. Res. 86, 389–404, 1981.

[2] D.C. Rubie, The olivine → spinel transformation and the rheology of subducting lithosphere, Nature 308, 505–508, 1984.

[3] S. Karato, Phase transformations and the rheological properties of mantle minerals, In: Earth's Deep Interior (the Doornbos Volume), D. Crossley and A.M. Soward, eds., in press, Gordon and Breach, 1997.

[4] E. Ito and H. Sato, A seismicity in the lower mantle by superplasticity of the descending slab, Nature 351, 140–141, 1991.

[5] H.W. Green II and P.C. Burnley, A new self-organizing mechanism for deep-focus earthquakes, Nature 341, 733–737, 1989.

[6] M.R. Riedel and S. Karato, Microstructural development during nucleation and growth, Geophys. J. Int. 125, 397–414, 1996.

[7] S.H. Kirby, Rheology of the lithosphere, Rev. Geophys. Space Phys. 21, 1458–1487, 1983.

[8] S. Karato, Plasticity–crystal structure systematics in dense oxides and its implications for the creep strength of the Earth's deep interior: A preliminary result, Phys. Earth Planet. Inter. 55, 234–240, 1989.

[9] M.R. Handy, Flow laws for rocks containing two non-linear viscous phases: a phenomenological approach, J. Struct. Geol. 16, 287–301, 1994.

[10] D.C. Rubie and C.R. Ross II, Kinetics of the olivine–spinel transformation in subducting lithosphere: experimental constraints and implications for deep slab processes, Phys. Earth Planet. Inter. 86, 223–241, 1994.

[11] D. P McKenzie, Speculations on the consequences and causes of plate motions, Geophys. J.R. Astron. Soc. 18, 1–32, 1969.

[12] D.P. McKenzie, Temperature and potential temperature beneath island arcs, Tectonophysics 10, 357–366, 1970.

[13] P. Molnar, D. Freedman and J.S.H. Shih, Lengths of intermediate and deep seismic zones and temperatures in downgoing slabs of lithosphere, Geophys. J.R. Astron. Soc. 56, 41–54, 1979.

[14] T. Lay, The fate of descending slabs, Annu. Rev. Earth Planet. Sci. 22, 33–62, 1994.

[15] D.C. Rubie, Y. Tsuchida, T. Yagi, W. Utsumi, T. Kikegawa, O. Shimomura, and A.J. Brearley, An in situ X-ray diffraction study of the kinetics of the Ni_2SiO_4 olivine–spinel transformation, J. Geophys. Res. 95, 15,829–15,844, 1990.

[16] K. Fujino and T. Irifune, TEM studies on the olivine to modified spinel transformation in Mg_2SiO_4, In: High Pressure Research: Application to Earth and Planetary Sciences, Y. Syono and M.H. Manghnani, eds., pp. 237–243, Terra, 1992.

[17] A.J. Brearley and D.C. Rubie, Transformation mechanisms of San Carlos olivine to β-phase under subduction zone conditions, Phys. Earth Planet. Inter. 86, 45–67, 1994.

[18] J.W. Christian, The theory of transformations in metals and alloys. Vol. I. Equilibrium and general kinetic theory, Pergamon, Oxford, 2nd ed., 1975.

[19] R. Däßler, D.A. Yuen, S. Karato and M.R. Riedel, Two-dimensional modeling of thermokinetic coupling and the consequences on the phase boundaries of subducting slabs, Phys. Earth Planet. Inter. 94, 217–239, 1996.

[20] J.W. Cahn, The kinetics of grain boundary nucleated reactions, Acta Metall. 4, 449–459, 1956.

[21] R. Däßler and D.A. Yuen, The effects of phase transition kinetics on subducting slabs, Geophys. Res. Lett. 20, 2603–2606, 1993.

[22] W.H. Press, B.P. Flannery, S.A. Teukolsky, and W.T. Vetterling, Numerical Recipes: The Art of Scientific Computing, Cambridge Univ. Press, Cambridge, 1989.

[23] D.T. Griggs, The sinking lithosphere and the focal mechanism of deep earthquakes, In: The Nature of the Solid Earth, E.C. Robertson, J.F. Hays and L. Knopoff, eds., pp. 361–384, McGraw-Hill, New York, NY, 1972.

[24] S.H. Kirby, S. Stein, E. Okal and D.C. Rubie, Metastable

mantle phase transformations and deep earthquakes in subducting oceanic lithosphere, Rev. Geophys. 34, 261–306, 1996.
[25] S. Karato, Grain-size distribution and rheology of the upper mantle, Tectonophysics 104, 155–176, 1984.
[26] S. Karato, M.S. Paterson and J.D. Fitz Gerald, Rheology of synthetic olivine aggregates: influence of grain size and water, J. Geophys. Res. 91, 8151–8176, 1986.
[27] S. Karato and P. Wu, Rheology of the Upper Mantle: A Synthesis, Science 260, 771–778, 1993.
[28] T.N. Tingle, H.W. Green II and R.S. Borch, High-temperature creep experiments on the olivine and spinel polymorphs of Mg_2GeO_4: implications for the rheology of the Earth's mantle, EOS Trans. AGU 72, 297, 1991.
[29] G.Y. Bussod, T. Katsura and D.C. Rubie, The large volume multi-anvil press as a high P–T deformation apparatus, Pure Appl. Geophys. 141, 579–599, 1993.
[30] C. Dupas, N. Doukhan, J.-C. Doukhan, H.W. Green II and T.E. Young, Analytical electron microscopy of a synthetic peridodite experimentally deformed in the β olivine stability field, J. Geophys. Res. 99, 15,821–15,832, 1994.
[31] C. Goetze and B. Evans, Stress and temperature in the bending lithosphere as constrained by experimental rock mechanics, Geophys. J.R. Astron. Soc. 59, 463–478, 1979.
[32] M.F. Ashby and R.A. Verrall, Micromechanisms of flow and fracture, and their relevance to the rheology of the upper mantle, Philos. Trans. R. Soc. London A 288, 59–95, 1977.
[33] Y. Okamoto, Creep deformation mechanisms in oxides and deformation of spinel ferrites, In: Rheology of Solids and of the Earth, S. Karato and M. Toriumi, eds., Chapt. 6, pp. 83–104, Oxford Sci. Publ., Oxford, 1989.
[34] G. Ranalli, Rheology of the Earth, Chapman and Hall, London, 2nd ed., 1995.
[35] V S. Solomatov and D.J. Stevenson, Can sharp seismic discontinuities be caused by non-equilibrium phase transformation?, Earth Planet. Sci. Lett. 125, 267–279, 1994.
[36] D.C. Rubie and A.J. Brearley, Mechanism of the $\gamma-\beta$ phase transformation of Mg_2SiO_4 at high temperature and pressure, Nature 348, 628–631, 1990.
[37] A.J. Brearley, D.C. Rubie and E. Ito, Mechanisms of the transformations between the α, β and γ polymorphs of Mg_2SiO_4 at 15 GPa, Phys. Chem. Miner. 18, 343–358, 1992.
[38] S.H. Kirby, Interslab earthquakes and phase changes in subducting lithosphere, Rev. Geophys. Suppl., US Natl. Rep. IUGG 1991–1994, pp. 287–297, 1995.
[39] L. Kerschhofer, T.G. Sharp and D.C. Rubie, Intracrystalline transformation of olivine to wadsleyite and ringwoodite under subduction zone conditions, Science 274, 79–81, 1996.
[40] S.H. Kirby and E. Okal, Geodynamic implications of deep earthquakes beneath the Fiji basin: Seismic failure in slabs stagnated in the mantle's transition zone, EOS Trans. AGU 77, 498, 1996.
[41] P.C. Burnley, H.W. Green II and D.J. Prior, Faulting associated with the olivine to spinel transformation in Mg_2GeO_4 and its implications for deep-focus earthquakes, J. Geophys. Res. 96, 425–443, 1991.
[42] S.H. Kirby, W.B. Durham and L.A. Stern, Mantle phase changes and deep-earthquake faulting in subducting lithosphere, Science 252, 216–225, 1991.
[43] D.L. Turcotte and G. Schubert, Geodynamics. Applications of Continuum Physics to Geological Problems, Wiley, New York, NY, 1982.
[44] M. Akaogi, E. Ito and A. Navrotsky, Olivine–modified spinel–spinel transitions in the system Mg_2SiO_4–Fe_2SiO_4: calorimetric measurements, thermochemical calculation, J. Geophys. Res. 94, 15,671–15,685, 1989.
[45] S. Karato, Rheological properties of materials composing the Earth's mantle, PhD Thesis, Univ. Tokyo, 1977.
[46] D.C. Rubie and A.J. Brearley, Phase transitions between β- and γ-$(Mg, Fe)_2SiO_4$ in the Earth's mantle; mechanisms and rheological implications, Science 264, 1445–1448, 1994.